Journal of Power Sources 229 (2013) 58–64

Contents lists available at SciVerse ScienceDirect

Journal of Power Sources

journal homepage: www.elsevier.com/locate/jpowsour

Ultrahigh oxygen reduction activity of Pt/nitrogen-doped porous carbon microspheres prepared via spray-drying

Ratna Balgis [a], Gopinathan M. Anilkumar [b], Sumihito Sago [b], Takashi Ogi [a,*], Kikuo Okuyama [a]

[a] Department of Chemical Engineering, Graduate School of Engineering, Hiroshima University, 1-4-1 Kagamiyama, Higashi-Hiroshima, Hiroshima 739-8527, Japan
[b] Research and Development Centre, Noritake Co., Ltd., 300 Higashiyama, Miyoshi, Aichi 470-0293, Japan

HIGHLIGHTS

- Pt/N-doped porous carbon was successfully synthesized via spray-drying method.
- Simultaneously modifying catalyst morphology during N-doping process.
- Pt NPs size was decreased with the increase of precursor pH.
- Ammonium hydroxide was used as N-doping agent.
- Ultrahigh ORR activity was recorded for a catalyst prepared at precursor pH 8.4.

GRAPHICAL ABSTRACT

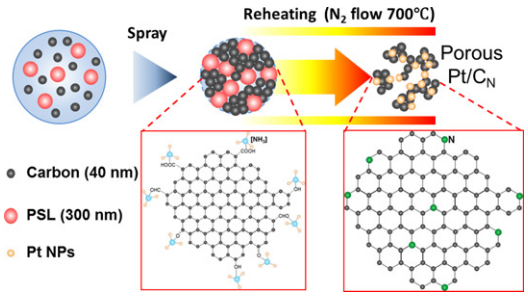

ARTICLE INFO

Article history:
Received 27 September 2012
Received in revised form
15 November 2012
Accepted 24 November 2012
Available online 12 December 2012

Keywords:
Spray drying
Oxygen reduction reaction
Nitrogen doped carbon
Pt nanoparticle
Electrocatalyst

ABSTRACT

Pt nanoparticles supported on nitrogen-doped porous carbon microspheres (Pt/C_N) were synthesized via an *in-situ* spray-drying technique followed by calcination. The addition of ammonium hydroxide had a remarkable influence on the solution chemistry, which promoted the simultaneous formation of metallic Pt and nitrogen doping onto carbon support material. Furthermore, the precursor pH influenced the subsequent oxygen reduction activity of the product. Ultrahigh oxygen reduction reaction (ORR) activity was recorded for a catalyst prepared at a precursor pH of 8.4 with mass activity and specific activity were 564 mA mg^{-1} Pt and 834 μA cm^{-2} Pt, respectively. This investigation resulted in an effective strategy to escalate the catalyst ORR during limited catalyst surface area enhancement.

1. Introduction

An energy source that is both cheap and eco-friendly is urgently needed to replace the current domination of fossil fuels such as petroleum and natural gas [1]. Polymer electrolyte membrane fuel cell (PEMFC) is considered to be one of the most promising candidates for a renewable power source, particularly for mobile and portable applications [2,3]. At the heart of a PEMFC, there is an active catalyst material used to accelerate electrochemical reactions, in which platinum-based materials are commonly used: platinum nanoparticles (Pt NPs), bimetallic-Pt NPs, and Pt NPs deposited on support materials [4–6].

Depositing Pt NPs on support materials is an effective strategy to reduce Pt utilization. However, in order to maintain the catalytic performance of a PEMFC at a sufficient level, the support materials require a high surface area and high electrical conductivity. From

* Corresponding author. Tel.: +81 82 424 7850; fax: +81 82 424 5494.
E-mail address: ogit@hiroshima-u.ac.jp (T. Ogi).

0378-7753/$ – see front matter © 2012 Elsevier B.V. All rights reserved.
http://dx.doi.org/10.1016/j.jpowsour.2012.11.143

this perspective, porous conductive materials (e.g., Carbon) are appropriate for use as a support material. In the previous study, we reported the enhancement of nanoparticle catalytic activity, by means of morphological control of porous carbon microspheres that influences the surface area of catalyst support [7]. A high ORR activity is absolutely desired for PEMFC electrodes, particularly for cathodic reactions [8]. However, the improvement of ORR activity by enhancing the surface area is constrained by the fact that an infinite amount of surface area is nonexistent.

The modification of carbon support materials is necessary to improve ORR activity. It is well known that the doping of nitrogen (N) into carbon support materials has a large impact on their oxygen reduction activity [8–11]. Generally, N-doped porous carbon materials can be synthesized by either "*in-situ*" or "*ex-situ*" methods. In the *in-situ* method, various types of N-contained hydrocarbons, e.g., acetonitrile, polypyrrole, polyacrylonitrile, or polyaniline, are used as a nitrogen source and usually synthesized by arc-discharge, laser ablation, chemical vapor deposition or solvothermal methods [12–16]. Meanwhile, the *ex-situ* method involves the passing of NH_3 gas at a high temperature to dope N onto the material [17,18].

In previous research, we found that any chemicals which can be decomposed into NH_3 at high temperature, such as urea, can be used as an N precursor [19]. Utilization of direct NH_3 gas of course attracts special attention due to its simplicity. However, this gas is categorized as a flammable one. Therefore, it is become a challenge to utilize other chemicals with lower risk and offer more advantages than as an N-doping agent only, such as ammonium hydroxide, which also can form NH_3 gas. Previously, our group successfully reduced nickel chloride into nickel particles using ammonium hydroxide without using a reducing agent [20,21]. To the best of our knowledge, the use of ammonium hydroxide as an N-doping agent of carbon had never been reported. Here, we report the role of ammonium hydroxide as an N-doping agent to enhance the overall ORR activity of the catalyst materials. In the present study, the formation of Pt NPs, doping of nitrogen, and morphology control of porous microsphere carbon were accomplished concurrently using an *in-situ* spray-drying method, which was safer than the other reported methods of nitrogen doping. A spray-drying technique has the potential for an industrial scale production to quickly obtain a homogenous particle morphology and chemical dispersion of the product [22,23]. Once the catalysts were prepared using the present method, they were examined for application to PEMFC.

2. Experimental

2.1. Preparation of Pt/C_N catalysts

First, two precursors were separately prepared. Precursor I was prepared by mixing an aqueous slurry of carbon black (0.224 wt.%, 40 nm, Mikuni Color Co., Ltd, Japan) with an aqueous slurry of anionic polystyrene latex (PSL, 0.3 wt.%, 300 nm) at a mass ratio of 1.3:1. Precursor II was prepared by adding ammonium hydroxide solution (28–30 wt.%, Kanto Chemical Co., Ltd, Japan) into an aqueous solution of chloroplatinic acid (10 wt.%, Noritake Co., Ltd, Japan) until the desired pH was reached. The pH value increased with the increment of ammonium hydroxide concentration. Precursors I and II were mixed with the mass ratio of carbon black and chloroplatinic acid kept at 4:1, and the final pH was then measured. The mixed precursor was spray-dried using a mini spray-dryer (BÜCHI B-290) at 180 °C with an air flow of 11.1 L min^{-1}. The sprayed composite catalysts were then calcined in 2 steps. First, the catalysts were calcined at 700 °C for 30 min, under a nitrogen atmosphere, followed by a second calcination at 300 °C for 30 min under an ambient atmosphere (See Supporting information 1).

2.2. Materials characterization

The morphology of the catalysts was observed using a field emission scanning electron microscope (FE-SEM, Hitachi, S-5000, 20 kV) and transmission electron microscopy (TEM, JEOL-JEM-2010, 200 kV). The Pt amount in the catalyst was measured using an inductively coupled plasma (ICP) mass spectrometer (SII, SPS-3000). The crystal structure was characterized by X-ray diffraction (XRD, Rigaku, RINT2000). The surface area was determined quantitatively using N_2 adsorption–desorption (BEL Japan, Inc., BELSORP-max), and was calculated using the Brunauer, Emmett, and Teller (BET) method.

2.3. Electrochemical characterization

Electrochemical characterization was performed using cyclic voltammetry (CV) and rotating disc electrode (RDE) (Hokuto Denko, HR-301). The catalyst ink was prepared by dispersing 18.5 mg of catalyst into a mixture of 6 mL isopropanol (Cica-reagent, Kanto Chemical Co. Inc., Japan) and 19 mL ultrapure water. A 15 μL of Nafion® dispersion solution (5 wt.%, Wako Pure Chemical Industries, Ltd., Japan) was added, then the mixture of catalyst ink was placed in an ice bath and sonicated for at least 30 min. 10 μL of catalyst ink was transferred onto a polished glassy carbon disk and allowed to dry in order to form a catalyst layer. The electrochemical measurement setup was similar to our previous report [4]. Briefly, the CV measurements were scanned between 0 and 1.2 V vs. RHE with a sweep rate of 100 mV s^{-1} using a fresh 0.1 M $HClO_4$ electrolyte solution. Nitrogen gas was flowed to the electrolyte solution for 30 min to de-oxygenate the environment. The saturation gas was switched to oxygen for RDE measurement. Rotation rates were controlled at 400, 900, 1600, 2500, and 3600 rpm to collect data for Koutecký–Levich plots. Measurements were carried out at 10 mV s^{-1} sweep rates in a typical polarization program of 0.2 V → 1.2 V. The background current was measured by running the oxygen reduction reaction (ORR) sweep profile without rotation in N_2-purged 0.1 M $HClO_4$ before the ORR measurement to eliminate any contributions of capacitive current.

3. Results and discussion

A set of experiments were performed to study the role of an ammonia solution in the formation of Pt NPs. Five precursors with and without the addition of an ammonia solution were prepared for spray-drying. For a precursor with no ammonia (S1), the mixture pH was measured at 1.0, meanwhile, for the precursors with addition of ammonia (S2, S3, S4, S5), pH was adjusted to be 2.2, 8.4, 10.3, and 12.8, respectively.

XRD patterns of the samples prepared from the precursors with a pH of 1, 2.2, 8.4, 10.3 and 12.8 are shown in Fig. 1(a–e), respectively. The diffraction peaks of Pt were clearly observed for all samples, at diffraction angles, 2θ, of 39°, 46°, and 68°, corresponding to the crystalline planes of (111), (200), and (220), respectively (JCPDS Card no. 4-0802). Platinum oxide (PtO) was formed from the precursor without ammonia (S1), as indicated by the diffraction peaks of PtO at 33.5° and 54.3° (Fig. 1(a), JCPDS Card no. 42-866). Those peaks disappeared when the ammonia solution was added to the precursor, as shown in Fig. 1(b–e). Xia et al. found that NH_3 gas obtained as the result of NH_4Cl decomposition may initially react with the intermediate metal oxide (NiO) to form metal (Ni) particles with H_2 gas subsequently generated by the NH_3 decomposition at high temperature [19,20]. In a similar manner, the addition of an ammonia solution also promoted the formation of Pt NPs. The sizes of Pt NPs were calculated to be 4.53, 4.01, 3.96, and 3.81 nm for S2, S3, S4, and S5, respectively (see Supporting

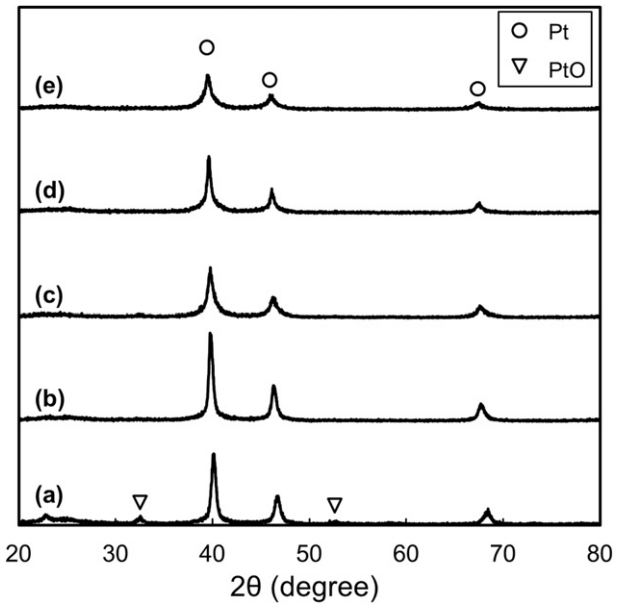

Fig. 1. XRD patterns for the Pt/C catalyst: (a) without pH adjustment at pH 1 (S1), (b) pH adjusted 2.2 (S2), (c) pH adjusted 8.4 (S3), (d) pH adjusted 10.3 (S4), and (e) pH adjusted 12.8 (S5).

information 2). It was apparent that the Pt size decreased with an increase in the pH of the precursor, which means that the number of $[H]^+$ ions in the precursor influenced the process of Pt reduction as well as that of Pt crystal growth. The increment of $[H]^+$ ion concentration was resulting the increase of Pt crystallite size. In addition, there is a critical level of concentration before $[H]^+$ ions will inhibit byproduct particles. Once the critical level is exceeded, a byproduct will be produced, which is PtO in the present study that was observed on sample S1. Since PtO formation was observed on S1, other analyses were carried out only for samples S2, S3, S4, and S5.

The structural properties of Pt/C_N catalysts were evaluated using nitrogen adsorption/desorption measurements. The adsorption–desorption isotherm curves of samples S2, S3, S4, and S5 are shown in Fig. 2(a–d). The isotherm curves characterized the initial rapid rise of gas volume absorbed as relative pressure was turned to a slow increase. The inflection point ($0.05 \leq P/P_0 \leq 0.3$) corresponded to both the completion of the monolayer coverage and the filling of the pores by capillary condensation. The rest of the curve corresponded to a normal multi-layer formation. These represent type II isotherm curves, which are usually encountered for nonporous particles or particles with pore diameters larger than micropores. No hysteresis could be found between the adsorption and desorption curves. Both of the curves overlapped completely across the entire relative pressure range. It was confirmed that the pores of the particles channeled one another and possibly formed hollow core-porous shell morphologies, which is ideal for a catalyst particle, due to the great support for the creation of a good three-phase boundary among the catalyst, the gas phase, and the electrolyte. The specific surface area can be obtained from this measurement, and summarized in Table 1.

The electrocatalytic activities of prepared Pt/C_N catalysts are represented in the CV and ORR polarization curves. The hydrogen adsorption and desorption characteristics of prepared catalysts at the 10th and 200th cycle measurements are shown in Fig. 3(a) and (b), respectively. All the CV curves show both the weak and the strong adsorption peaks of hydrogen ions, which were observed

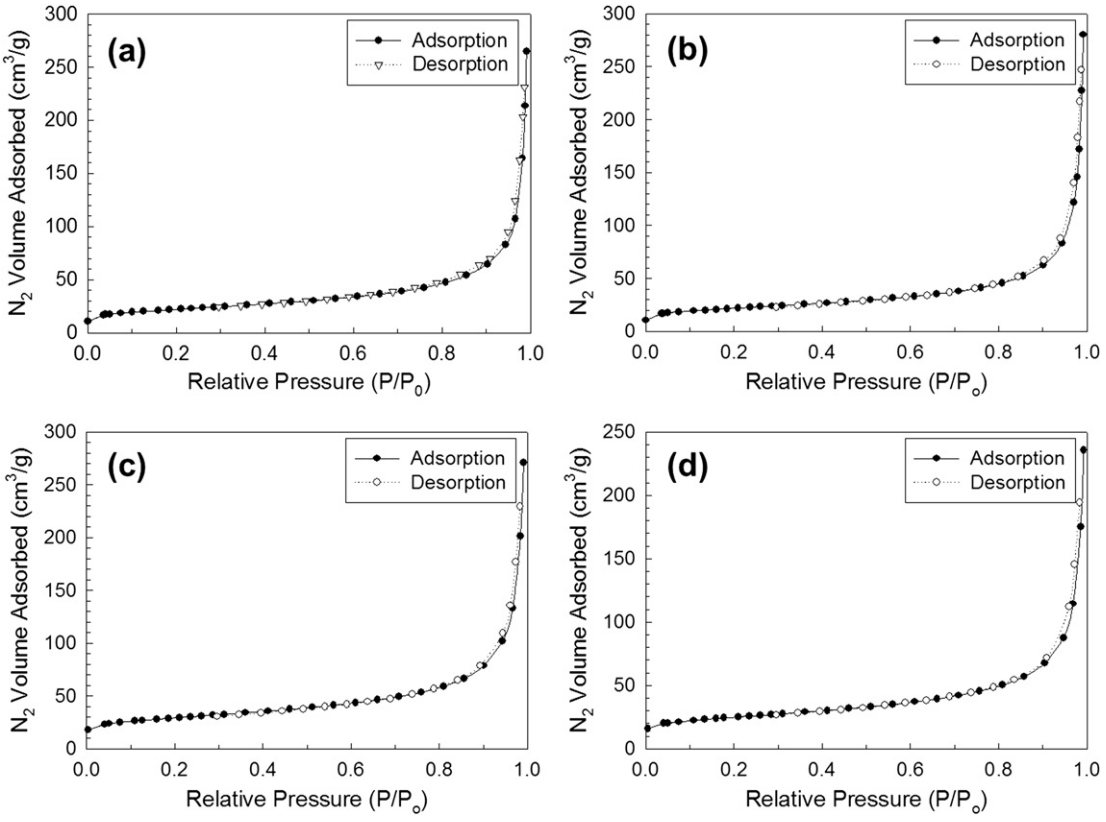

Fig. 2. Nitrogen adsorption–desorption isotherm curves of pH adjusted samples using ammonium hydroxide: (a) S2, (b) S3, (c) S4, and (d) S5.

Table 1
Surface structural parameters for Pt/C_N catalyst with pH adjustment using ammonium hydroxide.

Sample	pH	Particle size (μm)	SBET ($m^2\ g^{-1}$)
S2	2.2	3.5	78
S3	8.4	2.9	76.7
S4	10.3	2.7	103
S5	12.8	2.6	88.3

Table 2
Catalyst characterization results for the pH adjustment of Pt/C_N.

Sample	pH	Pt particle size (nm)	Pt loading (wt.%)	Pt amount on RRDE (μg Pt cm^{-2})	ECSA ($m^2\ g^{-1}$ Pt)	
					10 cycles	200 cycles
S2	2.2	4.53	23.38	8.79	50	45
S3	8.4	4.01	25.10	9.44	68	59
S4	10.3	3.96	21.27	8.00	50	50
S5	12.8	3.81	21.42	8.06	40	36

during the negative-going potential scan, and were assigned to weakly and strongly bonded hydrogen atoms, respectively. Corresponding desorption peaks of hydrogen ions also were observed during the reserve potential scan. In order to quantify the electrocatalytic activity of prepared catalysts, the electrochemically active surface area (ECSA) of Pt NPs was calculated using the hydrogen adsorption charge ($Q_{H\text{-adsorption}}$), which was limited by a minimum potential that was selected just above the potential of H_2 generation onwards. The ECSA of prepared samples at the 10th and 200th cycles are shown in Table 2.

A characteristic set of polarization curves for the ORR on the prepared Pt/C_N catalysts S2, S3, S4, and S5 is shown in Fig. 4(a). In order to examine figure of merit of prepared catalyst, the oxygen reduction reaction activity of commercial Pt/C catalyst (46.1 wt.%, purchased from Tanaka Kikinzoku Kogyo Co., Ltd.) was also measured under the same condition as that of the prepared Pt/C_N catalysts. The diffusion-limiting current density expected for materials that support a direct $4e^-$ transfer usually ranges between −5 and −6 mA cm^{-2}. These were obtained below 0.6 V with an electrode angular speed at 1600 rpm for all samples. The target potential for the calculation of the mass activity and specific activity was quantified at $E = 0.85$ V. Fig. 4(b) represents the Tafel plots derived from the kinetic currents of S2, S3, S4, S5, and commercial Pt/C. The mass activity and specific activity were evaluated from a Koutecký–Levich plot using the limiting current method, which was calculated by normalizing the Pt loading of the disk electrode; the specific activities were estimated by calculating the mass-specific activities and normalizing them to the Pt electrochemical surface area. The values for mass activity and specific activity of prepared samples and commercial Pt/C are shown in Fig. 4(c) and (d), respectively. The mass activity and specific activity of commercial Pt/C catalyst were slightly higher compared to S2, S4, and S5. However, it was more than half lower than that of the S3 sample. It is proven that the presence of N atom at carbon edges support the active site of catalyst. The ORR activity shows that there is an optimum amount of N-doping which was limited on the certain amount of $NH_3 \cdot H_2O$ addition until pH 8.4 was reached, at the higher amount of $NH_3 \cdot H_2O$ addition, the ORR activity of catalyst was tend to decrease due to the catalyst poisoning by the remaining NH_3 [24]. One can conclude that appropriate amount of N source addition to the S3 encountered the oxygen reduction reaction ability, while commercial Pt/C only relies on the ability of Pt active surface.

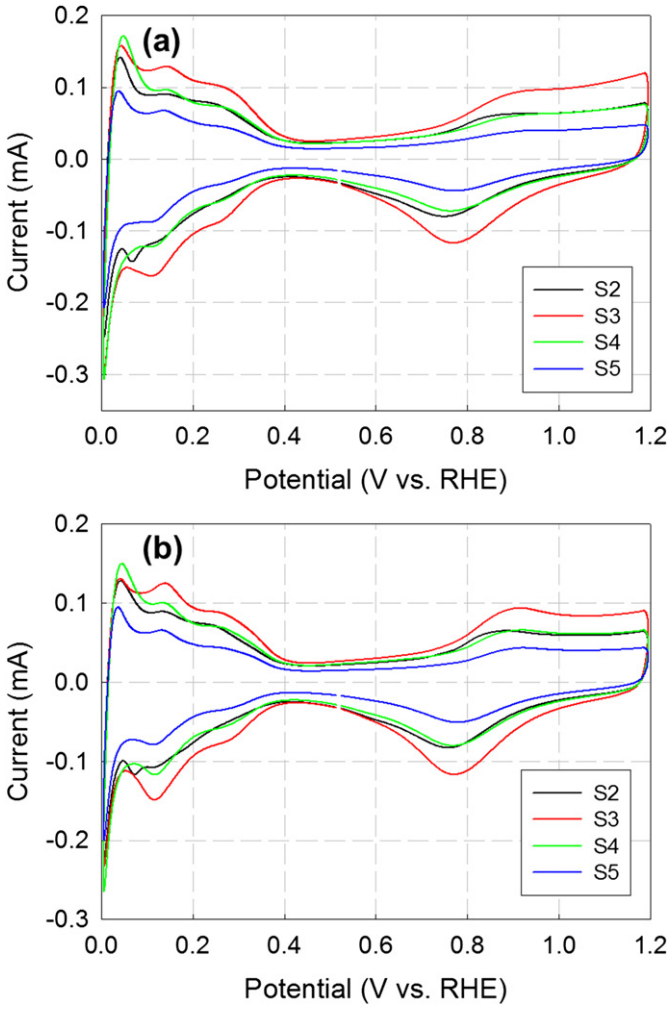

Fig. 3. Cyclic voltammograms of various pH adjusted catalyst samples in O_2-free 0.1 M $HClO_4$ (cycling between 0 and 1.2 V at 100 mV s^{-1} sweep rate) at: (a) 10 cycles and (b) 200 cycles.

The morphology of catalyst has an effect to electrocatalytic activity. Good dispersion of Pt NPs and the N from ammonia processing that was doped to the carbon support during heat treatment improved the ORR activity. The mechanism for the possible reactions from catalyst formation can be presented as follows:

$$NH_3 \cdot H_2O \leftrightarrow NH_4^+ + OH^- \quad (1)$$

$$OH^- + H^+ \leftrightarrow H_2O \quad (2)$$

With the addition of chloroplatinic acid, the mechanism for the possible reactions would be as follows:

$$2NH_4^+ + 2OH^- + H_2PtCl_6 \cdot xH_2O \rightarrow 2NH_4Cl + PtCl_4 + (x+2)H_2O \quad (3)$$

Precursor II further modified the carbon nanoparticles in precursor I during calcination at 700 °C for 30 min. The used carbon nanoparticles have various groups on the surface such as −COOH, −CHO, −C−OH, and −C═O (product data of Mikuni Co., Ltd.). As with the results from previous research [25], parts of the Pt ion could be adsorbed by carbon particles and reduced via the following two reactions:

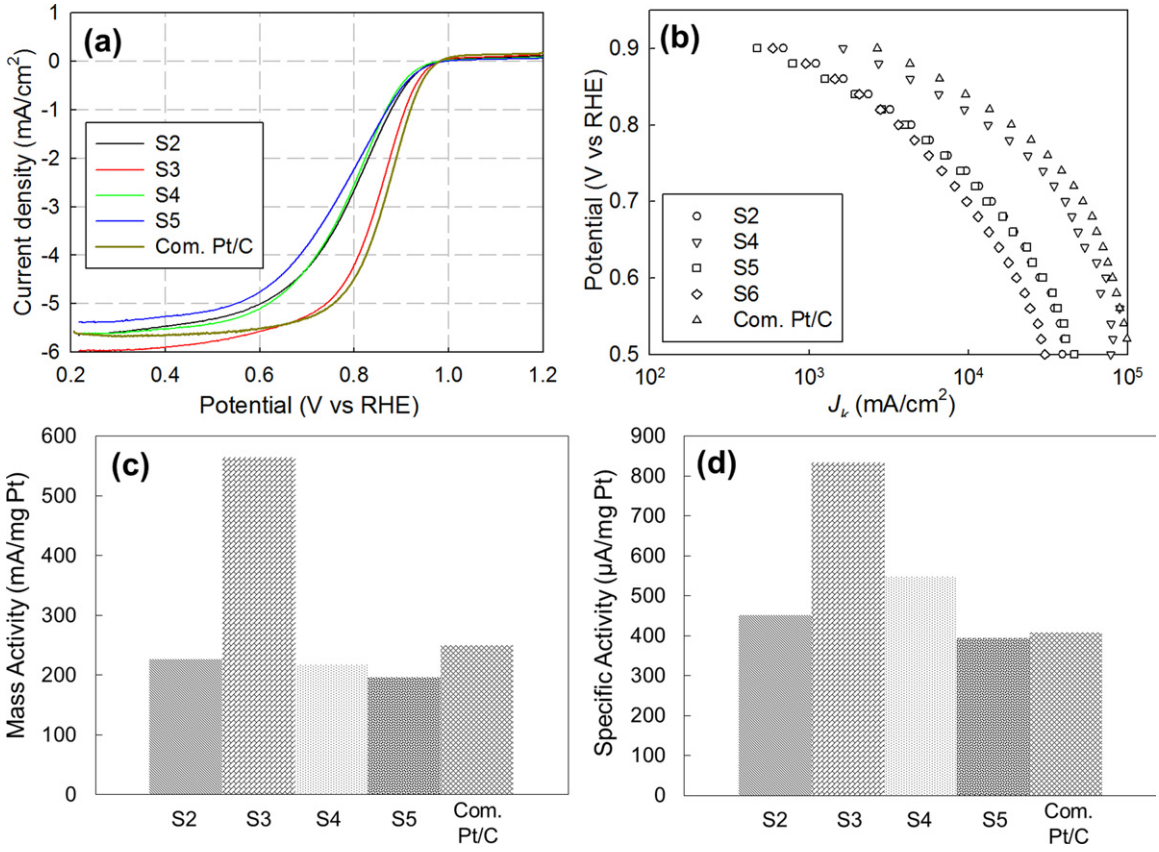

Fig. 4. (a) ORR polarization curves of S2, S3, S4, S5, and com. Pt/C in O_2 saturated 0.1 M $HClO_4$ at a sweep rate 10 mV s^{-1} and a rotation rate of 1600 rpm, (b) Tafel plots derived from the kinetic currents of the catalysts, (c) mass activities and (d) specific activities for the catalysts at 0.85 V (vs RHE).

$$-C-H + PtCl_4 + H_2O \rightarrow -C-OH + Pt(0,II) + H^+ \quad (4)$$

$$-C=O + PtCl_4 + H_2O \rightarrow -COOH + Pt(0,II) + H^+ \quad (5)$$

Reactions (4) and (5) emphasize the possibility of Pt (0) formation for the S1 sample, although PtO nanoparticles are still obtained due to the uncompleted reduction. For the other samples, the contained NH_4Cl will decompose into NH_3 and HCl gas at high temperature, and some of the NH_3 gas will decompose further into N_2 and H_2 gas. These two gases will also promote and accomplish the reduction process of Pt ions.

A schematic representation of the N-doping is presented in Fig. 5. The NH_3 molecule could easily get attached to the oxygen-containing functional groups in a carbon particle and be transformed to an N atom at the carbon edges and/or the defect sites at 300–700 °C [26]. The doping of N into carbon-based materials would enhance the catalytic activity toward an ORR [8–10],

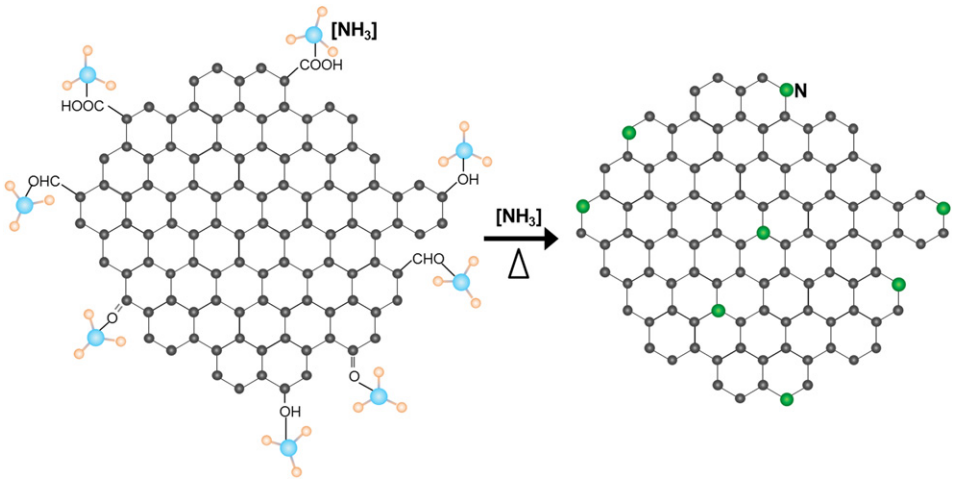

Fig. 5. Schematic illustration of the reaction pathway for the N-doping into a Pt/C catalyst.

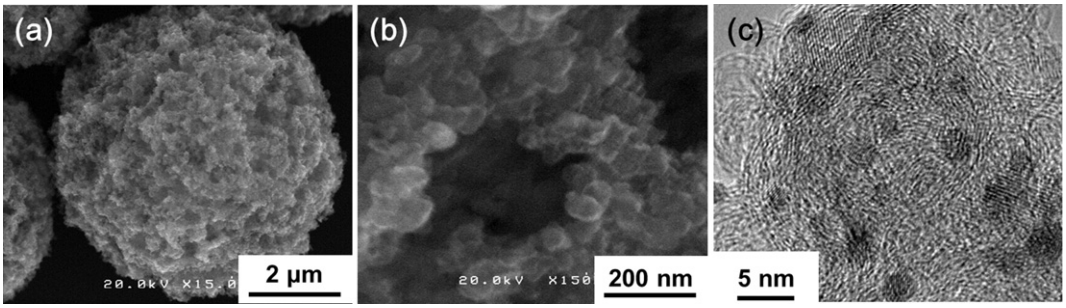

Fig. 6. (a & b) SEM images of S3 and (c) TEM images of Pt dispersion on the surface S3.

because the over-potential loss due to the slow reaction kinetics of an ORR is more than a quarter of the total ideal electrode potential, which greatly decreases the energy density of fuel cell. N-doped carbon as the catalyst support is also expected to improve the durability of the resultant catalyst, because of the enhanced π bonding and the basic properties of the strong electron donor behavior of N [27–31]. In addition, the presence of nitrogen merely indicated the presence of edge sites of graphene, as reported by Matter et al. [32].

As shown in Fig. 4(c) and (d), sample S3 had the highest ORR activity. The mass activity and specific activity of S3 were 564 mA mg^{-1} Pt, and 834 μA cm^{-2} Pt, respectively, which may have been due to the presence of an appropriate amount of N atoms doping into carbon as has been explained above. Here, we demonstrated that high value of specific activity can compensate even for high ECSA catalyst due to the high amount of mass activity, as a result of the presence of Pt and N atoms to conduct ORR. The substituted-nitrogen atoms gave advantageous on nucleation sites for Pt and finally enhance catalytic activity. A similar phenomenon also was reported elsewhere [33]. Therefore, we concluded that compared with the creation of a high surface area for catalyst support, the doping of N to the support materials had a larger impact on ORR activity. This also became one of the strategies used to overcome the limitations of catalyst surface area enhancement for the improvement of ORR activity.

Fig. 6 shows the FE-SEM and HR-TEM images of sample S3, and confirms that the morphology of prepared catalysts was that of a porous microsphere. The catalyst particles and their macropore sizes were measured from those images for more than 200 particles, and are tabulated in Table 1. The macropore size was relatively uniform for all samples (~180 nm); meanwhile, the particle size decreased with increments in pH of the precursor, which implies that a large droplet size is favorable for a solution containing a high concentration of $[H]^+$ ion. The dispersion of Pt NPs on the support material was confirmed by HR-TEM images (Fig. 6(c)). The chemical mapping of sample S3 in Fig. 7 shows that nitrogen and platinum

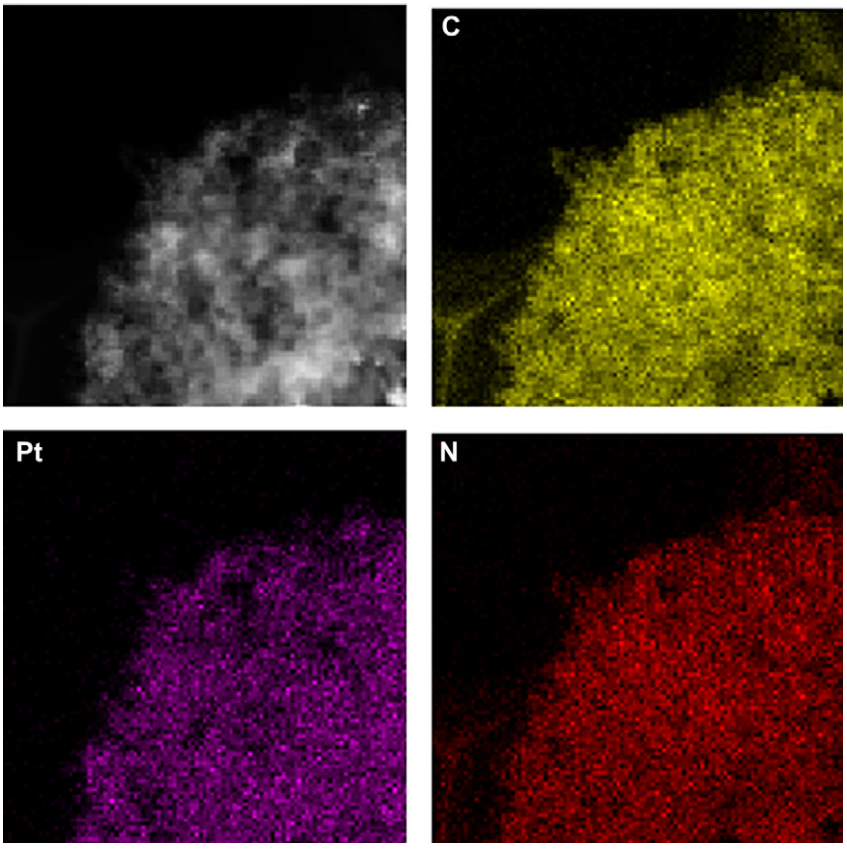

Fig. 7. Chemical mapping of S3.

were distributed very well on the carbon materials. This confirms the success of the present method to simultaneously dope N and form metal Pt on the structured morphology of carbon support materials, which is very suitable for industrial application.

4. Conclusion

In conclusion, the present study showed that the formation of Pt NPs and N-doping into structurally engineered carbon support materials was done simultaneously via a spray-drying method. Control of the Pt size and N-doping were done by simply adjusting the precursor pH using ammonium hydroxide. Designing catalyst support morphology with N-doping escalates the oxygen reduction reaction. Ultrahigh oxygen reduction activity was found at a precursor pH of 8.4 with mass and specific activities were 564 mA mg^{-1} Pt and 834 μA cm^{-2} Pt, respectively.

Acknowledgment

This research was supported by a grant in aid for Scientific Research (A) (No. 22246099) sponsored by the Ministry of Education, Culture, Sports, Science and Technology (MEXT) of Japan. The authors would like to thank Dr. A. B. Suryamas from Hiroshima University for valuable discussion and Dr. E. Tanabe from the Hiroshima Prefectural Institute of Industrial Science and Technology and Mr. M. Ito from the R&D center of Noritake Co., Ltd./JFCC, Japan, for helping with the TEM and chemical mapping analysis. R. B. thanks MEXT of Japan for a doctoral scholarship.

Appendix A. Supplementary data

Supplementary data related to this article can be found at http://dx.doi.org/10.1016/j.jpowsour.2012.11.143.

References

[1] J.-D. Qiu, G.-C. Wang, R.-P. Liang, X.-H. Xia, H.-W. Yu, J. Phys. Chem. C 115 (2011) 15639–15645.
[2] A. Esmaeilifar, S. Rowshanzamir, M.H. Eikani, E. Ghazanfari, Energy 35 (2010) 3941–3957.
[3] A. Morin, F. Xu, G. Gebel, O. Diat, Int. J. Hydrogen Energy 36 (2011) 3096–3109.
[4] B. Lim, M. Jiang, P.H.C. Camargo, E.C. Cho, J. Tao, X. Lu, Y. Zhu, Y. Xia, Science 324 (2009) 1302–1305.
[5] M. Shao, A. Peles, K. Shoemaker, Nano Lett. 11 (2011) 3714–3719.
[6] A. Chen, P. Holt-Hindle, Chem. Rev. 110 (2010) 3767–3804.
[7] R. Balgis, G.M. Anilkumar, S. Sago, T. Ogi, K. Okuyama, J. Power Sources 203 (2012) 26–33.
[8] Y. Shao, J. Sui, G. Yin, Y. Gao, Appl. Catal. B Environ. 79 (2008) 89–99.
[9] R. Kobayashi, J.-I. Ozaki, Chem. Lett. 38 (2009) 396–397.
[10] J.-I. Ozaki, S.-I. Tanifuji, A. Furuichi, K. Yabutsuka, Electrochim. Acta 55 (2010) 1864–1871.
[11] T. Palaniselvam, R. Kannan, S. Kurungot, Chem. Commun. 47 (2011) 2901–2912.
[12] Z. Lei, M. Zhao, L. Dang, L. An, A.-Y. Lo, N. Yu, A.-B. Liu, J. Mater. Chem. 19 (2009) 5985–5995.
[13] Y. Xia, R. Mokaya, Chem. Mater. 17 (2005) 1553–1560.
[14] C.M. Yang, C. Weidenthaler, B. Spliethoff, M. Mayanna, F. Schüth, Chem. Mater. 17 (2005) 355–358.
[15] A. Lu, A. Kiefer, W. Schmidt, F. Schüth, Chem. Mater. 16 (2004) 100–103.
[16] C. Xiao, W. Chu, Y. Yang, X. Li, X. Zhang, J. Chen, Biosens. Bioelectron. 26 (2011) 2934–2939.
[17] F. Jaouen, M. Lefévre, J.-P. Dodelet, M. Cai, J. Phys. Chem. B 110 (2006) 5553–5558.
[18] M. Lefèvre, J.-P. Dodelet, P. Bertrand, J. Phys. Chem. B 104 (2000) 11238–11247.
[19] T. Ogi, Y. Kaihatsu, F. Iskandar, W.-N. Wang, K. Okuyama, Adv. Mater. 20 (2008) 3235–3238.
[20] B. Xia, I.W. Lenggoro, K. Okuyama, J. Mater. Res. 15 (2000) 2157–2166.
[21] B. Xia, I.W. Lenggoro, K. Okuyama, J. Mater. Sci. 36 (2001) 1701–1705.
[22] R. Balgis, F. Iskandar, T. Ogi, A. Purwanto, K. Okuyama, Mater. Res. Bull. 46 (2011) 708–715.
[23] A.B.D. Nandiyanto, K. Okuyama, Adv. Powder Technol. 22 (2011) 1–19.
[24] Y. Wang, K.S. Chen, J. Mishler, S.C. Cho, X.C. Adroher, Appl. Energy 88 (2011) 981–1007.
[25] S. Chen, R. Xu, H. Huang, J. Mater. Sci. 42 (2007) 9572–9581.
[26] Z. Mou, X. Chen, Y. Du, X. Wang, P. Yang, S. Wang, Appl. Surf. Sci. 258 (2011) 1704–1710.
[27] Y.Y. Shao, G.P. Yin, Y.Z. Gao, P.F. Shi, J. Electrochem. Soc. 153 (2006) A1093–A1097.
[28] V.V. Strelko, V.S. Kuts, P.A. Thrower, Carbon 38 (2000) 1499–1503.
[29] M. Terrones, P. Redlich, N. Grobert, S. Trasobares, W.K. Hsu, H. Terrones, Y.Q. Zhu, J.P. Hare, C.L. Reeves, A.K. Cheetam, M. Ruhle, H.W. Kroto, D.R.M. Walton, Adv. Mater. 11 (1999) 655–658.
[30] S. van Dommele, K.P. de Jong, J.H. Bitter, Chem. Commun. (2006) 4859–4861.
[31] R. Czerw, M. Terrones, J.C. Charlier, X. Blase, B. Foley, R. Kamalakaran, N. Grobert, H. Terrones, D. Tekleab, P.M. Ajayan, W. Blau, M. Ruhle, D.L. Caroll, Nano Lett. 1 (2001) 457–460.
[32] P.H. Matter, L. Zhang, U.S. Ozkan, J. Catal. 239 (2006) 83–96.
[33] N. Kristian, X. Wang, Electrochem. Commun. 10 (2008) 12–15.